Springer Proceedings in Materials

Jiang Guo
Alam Md. Mahbub
Ying-Ren Chien *Editors*

Proceedings of the 9th International Conference on Mechanical Manufacturing Technology and Material Engineering

Volume 3

Springer

Springer Proceedings in Materials 76

Springer Proceedings in Materials publishes the latest research in Materials Science and Engineering presented at high standard academic conferences and scientific meetings. It provides a platform for researchers, professionals and students to present their scientific findings and stay up-to-date with the development in Materials Science and Engineering. The scope is multidisciplinary and ranges from fundamental to applied research, including, but not limited to:

- Structural Materials
- Metallic Materials
- Magnetic, Optical and Electronic Materials
- Ceramics, Glass, Composites, Natural Materials
- Biomaterials
- Nanotechnology
- Characterization and Evaluation of Materials
- Energy Materials
- Materials Processing

To submit a proposal or request further information, please contact one of the following Springer Publishing Editors according to your affiliation location:

European countries: **Mayra Castro** (mayra.castro@springer.com)
India, South Asia and Middle East: **Swati Meherishi** (swati.meherishi@springer.com)
South Korea: **Smith Chae** (smith.chae@springer.com)
Southeast Asia, Australia and New Zealand: **Ramesh Nath Premnath** (ramesh.premnath@springer.com)
The Americas: **Michael Luby** (michael.luby@springer.com)
China and all the other countries or regions, as well as topics in materials chemistry: **Maggie Guo** (maggie.guo@cn.springernature.com)

This book series is indexed in **SCOPUS** and **EI Compendex** database.

Jiang Guo · Alam Md. Mahbub · Ying-Ren Chien
Editors

Proceedings of the 9th International Conference on Mechanical Manufacturing Technology and Material Engineering

Volume 3

Springer

Editors
Jiang Guo
Dalian University of Technology
Dalian, Liaoning, China

Alam Md. Mahbub
Harbin Institute of Technology
Shenzhen, China

Ying-Ren Chien
National Ilan University
Yilan City, Taiwan

ISSN 2662-3161 ISSN 2662-317X (electronic)
Springer Proceedings in Materials
ISBN 978-981-96-5349-2 ISBN 978-981-96-5350-8 (eBook)
https://doi.org/10.1007/978-981-96-5350-8

This Springer imprint is published by the registered company Springer Nature Singapore Pte Ltd.
The registered company address is: 152 Beach Road, #21-01/04 Gateway East, Singapore 189721, Singapore

Preface

Welcome to the proceedings of the 9th International Conference on Mechanical Manufacturing Technology and Material Engineering (MMTME 2024). This prestigious event, held in Wuhan, China, from August 2 to 4, 2024, brings together scholars, researchers, industry professionals, and other delegates from around the globe to discuss the latest advancements, challenges, and future trends in mechanical manufacturing technology and material engineering.

The theme of MMTME 2024 revolves around fostering academic exchanges, broadening research horizons, enhancing academic research and exploration, and promoting the exchange of academic achievements and industrial cooperation. This conference aims to propel the high-quality development of the mechanical manufacturing industry and the field of material engineering. It serves as a platform for sharing insights, exploring innovative ideas, and strengthening collaborations among participants.

The proceedings of MMTME 2024 encapsulates a wide array of research papers that delve into the intricacies of mechanical manufacturing technology and material engineering. It delves into the forefront of research in areas like additive manufacturing, smart manufacturing systems, and innovative material solutions, addressing the current gaps and technological challenges within the industry. The content is structured to highlight significant innovations that are poised to redefine manufacturing processes, enhance material performance, and drive sustainability in production. Key topics such as the integration of AI and IoT in manufacturing, advancements in 3D and 4D printing technologies, and the development of new sustainable materials are explored. These are critical for pushing the boundaries of what's possible in manufacturing and materials science today.

The papers in this collection have undergone a rigorous review process to ensure their quality and relevance. Each submission was evaluated by at least two to three peer reviewers for its originality, technical content, depth of research, relevance to the conference theme, contribution to the field, and readability. The acceptance of these papers reflects the high standards of academic excellence that MMTME 2024 strives to uphold.

One of the highlights of MMTME 2024 is the presence of esteemed keynote speakers and chair professors, such as Professor Hakim Naceur from the Polytechnic University Hauts-de-France and Professor Jiang Guo from Dalian University of Technology. Their speeches and presentations have enriched the conference with valuable insights and perspectives on computational mechanics, additive manufacturing, and other forefront topics. In addition to the keynote speeches, the conference also features numerous sessions dedicated to specific topics, encouraging in-depth discussions and exchanges among participants. These sessions have fostered a vibrant and collaborative atmosphere, where ideas were freely shared, and innovative solutions were explored.

This paper volume is significant as it not only encapsulates state-of-the-art research but also provides a vision for future directions in the field. It sets out to solve problems

related to efficiency, cost-effectiveness, and environmental impact in manufacturing, offering new perspectives and solutions to researchers and professionals. It is also a testament to the dedication and hard work of the authors, reviewers, and organizers.

We hope that the proceedings of MMTME 2024 will inspire further research and collaboration, leading to new breakthroughs and innovations in these critical areas. Our heartfelt thanks go to all the authors, reviewers, speakers, sponsors, and participants who made MMTME 2024 a resounding success. Look forward to welcoming you to our future conferences, continuing the tradition of academic excellence and innovation.

The Committee of MMTME 2024

Committee Member

Conference General Chair

Prof. Hakim Naceur, Polytechnic University Hauts-de-France, France
Prof. Jiang Guo, Dalian University of Technology, China

Program Committee Chair

Prof. Yongsheng Ma, Southern University of Science and Technology, China

Publication Chair

Prof. Alam Md. Mahbub, Shenzhen Graduate School of Harbin Institute of Technology, China
Prof. Ying-Ren Chien, National Ilan University, China

Organizing Committee Chair

Prof. Xinyu Li, Huazhong University of Science and Technology, China

International Technical Program Committee

Prof. Richard (Chunhui) Yang, Western Sydney University, Australia
Prof. Jinliang Luo, University of South China, China
Prof. Youwei He, University of South China, China
Prof. Yusri Yusof, Unversiti Tun Hussein Onn Malaysia, Malaysia
Prof. Dr. Murat Tolga OZKAN, Gazi University, Turkey
Prof. Yudong Zhang, University of Leicester, UK
Prof. Yajun Liu, South China University of Technology, China
Prof. Prashanth Konda Gokuldoss. Tallinn University of Technology, India
Assoc. Prof. Junjun Lei, Guangdong University of Technology, China
Assoc. Prof. Xiaoyan Zhou, China University of Petroleum, China
Assoc. Prof. Xiaoming Kang, University of South China, China
Assoc. Prof. Biao Wang, Soochow University, China

Assoc. Prof. Venkata Siva Rama Prasad, St. Peters Engineering College (Autonomous), India
Assoc. Prof. Engin Derya Gezer, Karadeniz Technical University, Turkey
Researcher Denis Andrienko, Max Planck Institute for Polymer Research, Germany
Researcher Qinghua Liu, University of Science and Technology of China, China
Assistant Researcher Yiping Gao, Huazhong University of Science and Technology, China
Dr. Chunjiang Zhang, Huazhong University of Science and Technology, China
Dr. AHMED LEGROURI. International University of Grand-Bassam, Morocco
Dr. Hock Jin Quah, Universiti Sains Malaysia, Malaysia

Contents

Intelligent Mechanical System Design and Control

Intelligent Mechanical System Design and Control

Multi-Objective Optimization Design of Rear Seat of a Passenger Car Based on Multi-Criteria Decision-Making Approach

Hengliang Jiang, Xuan Zhou, and Jiangqi Long(✉)

Wenzhou University, Wenzhou 325035, Zhejiang, China
jqlong@wzu.edu.cn

Abstract. The optimized lightweight design of automotive seats has increasingly attracted the interest of researchers. A multi-objective optimization design was conducted for the rear seat of a passenger car. First, a finite element model of the rear seat luggage compartment collision was constructed and verified through physical tests. Then, the optimized Latin hypercube experimental design was combined with a multi-criteria decision-making method to conduct the multi-objective optimization of the rear seat. The optimized rear seat demonstrated slight performance improvements, along with reductions in cost and mass by 11.13% and 21.39%, respectively.

Keywords: Car seat frame · Lightweight optimization · Multi-Objective Optimization · multi-criterion decision making

1 Introduction

The optimization design of automotive seat structures is a significant area of research in the modern automotive industry. By employing optimization techniques, the overall quality of the seat can be improved, material utilization can be made more efficient, manufacturing costs can be lowered, and safety performance can be maintained. Additionally, ride comfort can be significantly enhanced, thereby improving the user experience. As a result, the optimization design of automotive seats has attracted considerable attention from researchers both domestically and internationally.

In this context, Zhou et al. [1] utilized GARS and NSGA-III optimization algorithms to improve the multi-objective design of a passenger car's rear seat frame, leading to enhanced seat performance, better economy, and lighter weight. Shan et al. [2] utilized grey relational analysis and the optimized coefficient of variation method to comprehensively assess the safety and lightweight characteristics of automotive seats under various working conditions, conducting a detailed comparative analysis with multi-criteria decision-making methods. Dai et al. [3] employed a large number of sample points simultaneously to construct a response surface method (RSM) approximation model using optimized Latin hypercubic design of experiments. Subsequently, they integrated

J. Guo et al. (Eds.): MMTME 2024, 76, pp. 3–11, 2025.
https://doi.org/10.1007/978-981-96-5350-8_1

this model with the NSGA-II optimization algorithm to optimize the lightweight design of the seat skeleton.

In summary, the lightweight design of automobile seats can eliminate excessive redundancy, thereby reducing production costs and improving efficiency. In the long term, it can effectively decrease automobile fuel consumption, lower tailpipe emissions, and promote energy savings and environmental protection, having a far-reaching impact.

2 Modeling and Verification

Table 1. Analysis of experimental and simulation errors.

Max X-Displacement	Simulation (mm)	Experiment (mm)	Error (%)
D_1	75.23	78.35	3.98
D_2	62.47	66.71	6.36

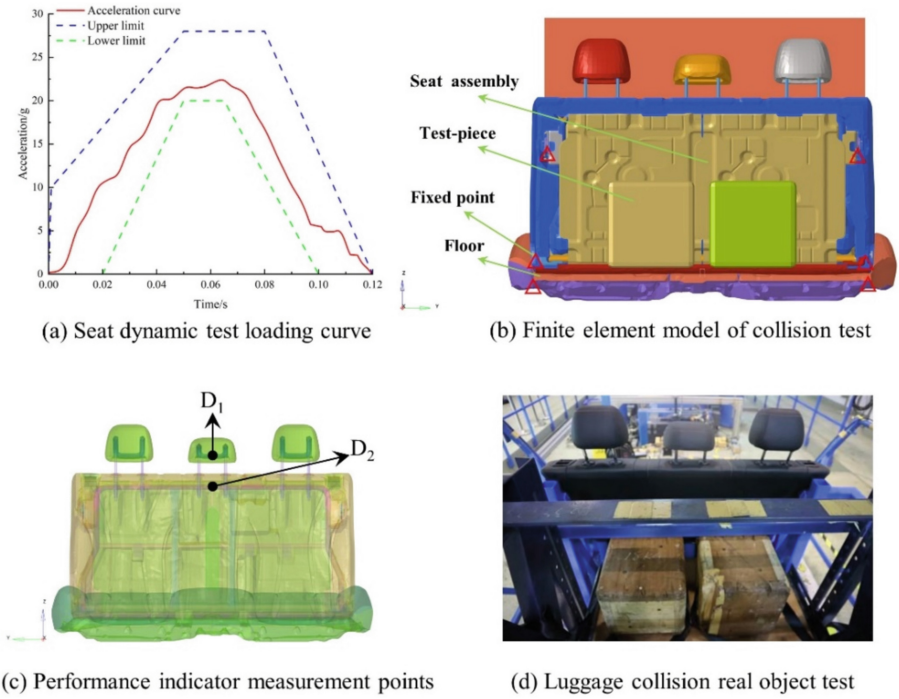

(a) Seat dynamic test loading curve

(b) Finite element model of collision test

(c) Performance indicator measurement points

(d) Luggage collision real object test

Fig. 1. Analysis diagram of passenger car rear seat luggage collision.

Figure 1 depicts the methodology used in a luggage collision test conducted on a passenger car's rear seat. In line with GB15083–2019 standards, a rear seat assembly and two test specimens, each measuring 300 mm × 300 mm × 300 mm with a 20 mm edge

chamfer and weighing 18 kg, were positioned on the trolley test bench. The acceleration-time curve shown in Fig. 1(a) was subsequently applied to simulate a collision scenario. Figure 1(c) captures a specific moment of impact of the rear seat during the collision test. The finite element model for the collision test was constructed using HyperMesh and analyzed with LS-DYNA, as illustrated in Fig. 1(b). Measurement points for headrest and backrest performance, as shown in Fig. 1(c), serve as the targets for optimizing safety performance. Compliant with GB15083–2019 standards, the finite element model incorporates two planes that ensure the headrest and backrest do not extend beyond 150mm and 100mm from the R-point, respectively. Measurements from HyperMesh indicate X-distances of 456mm and 430mm for the respective points, as shown in Fig. 1(c). Table 1 presents the maximum X-direction deformations observed in the simulations and actual tests, with a maximum error of no more than 7%, which is well within the safety limits defined by the 456 mm and 430 mm distances. This demonstrates the credibility of the FEA model used in this study for further design optimisation. Therefore, the optimised design results based on this FEA model can be considered reliable.

3 Optimization Process

This section focuses on the lightweight optimized design of the rear seat.

3.1 Optimization Strategy

This optimisation strategy integrates the optimal Latin Hypercube experimental design (OLHD) with the multi-criteria decision-making method for the multi-objective optimisation of rear seats in passenger car, as detailed in Fig. 2.

3.2 Selection of Design Variables and Responses

In the event of a frontal collision, the rear luggage compartment of a vehicle is subjected to a forward impact due to inertia. Therefore, the luggage compartment crash test assesses the structural integrity of the rear seatback structure. Thickness and material are used as design variables, as the thickness of different components and the type of steel (which varies in price from one steel to another) can have a significant impact on the lightweight design of the seatback structure, the overall performance of the seatback, and its economy. This study simplifies the tubes and plates comprising the backrest and headrest skeleton structures into six sets of optimized components, as illustrated in Fig. 2(a). The design variables for this optimization include the thickness and material grades of these components, labeled $T_1 \sim T_6$ and $M_1 \sim M_6$ in Fig. 3(a), amounting to a total of 12 variables. Table 2 lists the mechanical properties of the selected materials, encompassing yield strength (YS), elongation after break (E), ultimate tensile strength (UTS), and material cost (MC). The value ranges for the pertinent design variables are detailed in Table 3. Notably, this study defines the thickness variable as a continuous discrete variable in 0.1mm increments, corresponding to the manufacturable part's thickness. Regarding material variable processing, this study configures the material ID within the.k file and designates it as a variable for the relevant component. The value

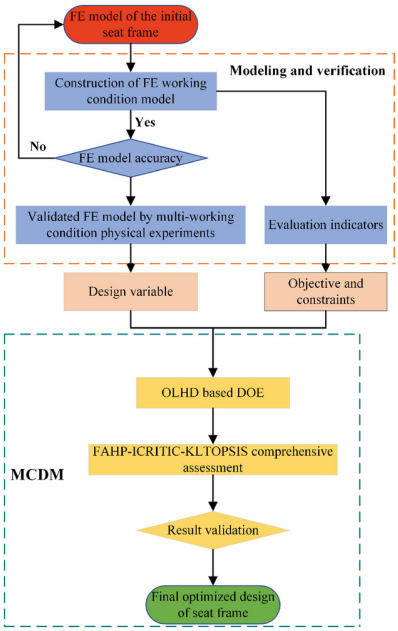

Fig. 2. Optimization strategy.

ranges for the pertinent design variables are presented in Table 3. Notably, this study defines the thickness variable as a continuous discrete variable at intervals of 0.1mm, reflecting the manufacturable part's thickness. Regarding material variable processing, the material ID is specified within the.k file, with this ID then designated as a variable for the respective part.

In summary, the design variables for this study include the thickness and material of backrest skeleton components. The responses encompass maximum X-displacement at measurement points D_1 and D_2, denoted as Dis_1 and Dis_2, respectively, material cost (*Cost*), total backrest skeleton weight (*Mass*). Specifically, Dis_1 and Dis_2 serve as safety evaluation indices, *Cost* represents economic considerations, and *Mass* corresponds to the lightweight objective, defining the optimization goals for this analysis. The contribution of the design variables to the four objective responses is calculated using the contribution analysis method described in the literature [3], as shown in Fig. 2(b). The figure indicates that the degree of influence of the 12 design variables on each of the four optimisation objective responses is primarily determined by the thickness variable, which has the highest influence, followed by the material variable.

3.3 Design of Experiments

In the previous study, quality, cost, and maximum deformation of critical parts were established as the optimization objectives for the multi-objective optimization design

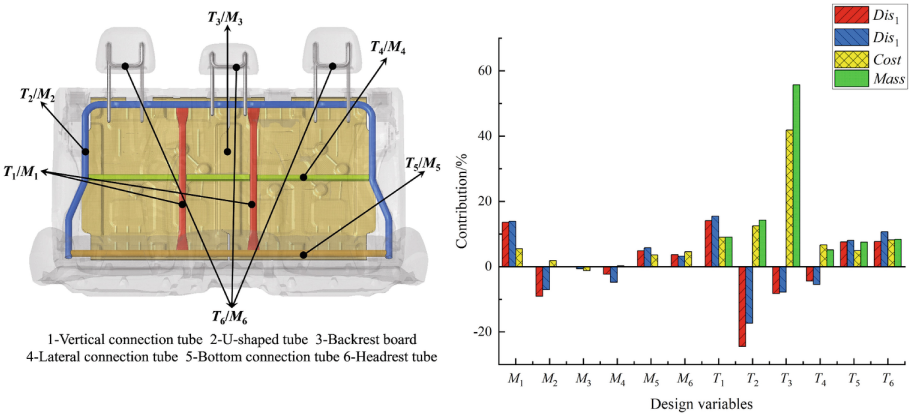

(a) (b)

Fig. 3. (a) Information on the spatial layout distribution of design variables; (b) Contribution values of design variables for optimization objectives.

Table 2. Analysis of experimental and simulation errors.

Material No	Material Name	YS (MPa)	UTS (MPa)	E (%)	MC (¥/kg)
101	DC04	165	372.6	32.2	5.18
102	DC01	172	451.4	35.8	4.28
103	SAPH370	225	492.1	28.5	4.71
104	SAPH400	255	528	27.8	4.92
201	Q235 TUBE	300	639.8	35.4	4.67
202	SAPH400	374.75	653.7	30.8	4.75
203	Q345 TUBE	455.5	625.8	25.1	5.22
204	QSTE420TM	459.7	691.6	25.3	5.65
301	B410LA	530	759	27.8	5.56
302	S650MC	650	814	9.5	5.82
303	HC700LA	700	899.25	8.6	6.21
304	20CrMnTi	835	1188	9.5	6.68

of a passenger car's rear seat. Thirty sets of sample points for multi-criteria decision-making were collected using the optimal Latin hypercube sampling method [4] commonly applied in engineering. The optimal solution was subsequently selected based on the decision ranking. The selected test sample data are presented in Table 4.

Table 3. Types and spatial ranges of design variables.

Variables	Type	Min	Baseline	Max	Increment	Resolution
T_1	Continuous	1.0	1.5	1.8	0.1	9
T_2	Continuous	1.0	1.5	1.8	0.1	9
T_3	Continuous	0.8	1.2	1.6	0.1	9
T_4	Continuous	0.8	1.2	1.6	0.1	9
T_5	Continuous	1.4	1.8	2.2	0.1	9
T_6	Continuous	1.0	1.5	1.8	0.1	9
M_1	Discrete	301	302	304	1	4
M_2	Discrete	201	203	204	1	4
M_3	Discrete	101	102	104	1	4
M_4	Discrete	301	301	304	1	4
M_5	Discrete	201	203	204	1	4
M_6	Discrete	201	203	204	1	4

Table 4. Types and spatial ranges of design variables.

No.	Variables							Responses			
	T_1/mm	$\cdots$	T_6/mm	M_1	$\cdots$	M_6		Dis_1	Dis_2	$Cost$	$Mass$
1	1.4	$\cdots$	1.3	304	$\cdots$	202		82.97	64.14	58.12	11.51
2	1.5	$\cdots$	1.8	301	$\cdots$	203		75.57	61.93	48.31	9.35
3	1.6	$\cdots$	1.4	301	$\cdots$	201		76.06	61.25	47.66	9.57
4	1.3	$\cdots$	1.8	304	$\cdots$	204		86.85	68.11	59.26	11.3
5	1.1	$\cdots$	1.4	301	$\cdots$	203		66.5	57.02	57.06	11.5
6	1.5	$\cdots$	1.5	303	$\cdots$	203		76	62.76	64.75	12.81
$\vdots$	$\vdots$	$\vdots$	$\vdots$	$\vdots$	$\vdots$	$\vdots$		$\vdots$	$\vdots$	$\vdots$	$\vdots$
30	1.4	$\cdots$	1.1	302	$\cdots$	203		73.05	60.05	60.24	12.3

3.4 Multi-Criteria Decision-Making Method

A reasonable weight relationship is fundamental to multi-criteria decision analysis. The current weight calculation methods include subjective weight, objective weight, and combination weight. Subjective weights can comprehensively consider the influence of various factors, offering high flexibility and adaptability. However, they are easily affected by the subjective preferences of decision makers, making it difficult to scientifically measure the importance of indicators. In contrast, objective weights, based on the relationship between data, have a higher degree of objectivity and scientific validity.

However, objective weighting often ignores the subjective intentions of decision makers, resulting in decisions that do not match the actual situation. To avoid the subjectivity and one-sidedness of weight calculation and achieve a balance of subjectivity and objectivity, this paper adopts the principle of minimum entropy to combine the weights obtained by the fuzzy analytic hierarchy process (FAHP) method and the improved criteria importance through inter-criteria correlation (ICRITIC) method. This approach yields a more accurate and reliable combination of weights. To better evaluate multiple design options, this paper proposes the FAHP-ICRITIC-KLTOPSIS method for multi-criteria decision analysis, incorporating the "KLTOPSIS" decision-making method cited in the literature [1]. The specific calculation process is as follows:

Step 1: Calculate the subjective weight factor vector w_i of each sub-objective using the FAHP method [3]; derive the objective weight factor vector w_i' of sub-objectives based on the ICRITIC method [5]. The weight calculation method is detailed in literature [3] and [5], and will not be elaborated on here due to space constraints.

Step 2: Combine the subjective and objective weights using the principle of minimum discriminatory information to align them as closely as possible, and define the objective function as follows:

$$\begin{cases} \min F(w) = \sum_{i=1}^{n} \left(w_i \ln \frac{w_i}{w_i'} \right) \\ s.t. \sum_{i=1}^{n} w_i = 1, w_i \geq 0, i = 1, 2, \cdots, n \end{cases} \tag{1}$$

Step 3: Following the "KLTOPSIS" calculation method described in the literature [1], the relative closeness of each alternative is calculated. The ranking of each alternative is then determined based on the magnitude of the relative closeness. The most significant improvement of the TOPSIS method in KLTOPSIS is the use of the Kullback-Leibler distance instead of the Euclidean distance to calculate the closeness of the positive and negative ideal solutions, with the final calculation being the relative closeness. The relevant computations are as follows:

$$\begin{cases} D_{i_{KL}}^{+} = \sqrt{\sum_{j=1}^{n} \left(z_j^{+} \log \frac{z_j^{+}}{z_{ij}} + \left(1 - z_j^{+}\right) \log \frac{1 - z_j^{+}}{1 - z_{ij}} \right)} \\ D_{i_{KL}}^{-} = \sqrt{\sum_{j=1}^{n} \left(z_j^{-} \log \frac{z_j^{-}}{z_{ij}} + \left(1 - z_j^{-}\right) \log \frac{1 - z_j^{-}}{1 - z_{ij}} \right)} \end{cases} \tag{2}$$

$$C_i = \frac{D_{i_{KL}}^{-}}{D_{i_{KL}}^{+} + D_{i_{KL}}^{-}}$$

where $D_{i_{KL}}^{+}$ and $D_{i_{KL}}^{-}$ represent positive and negative ideal solutions, respectively. C_i represents the relative closeness of each solution to the ideal solution.

The weights derived through various methods are presented in Table 5. Figure 4 shows that the 20th group of solutions is the optimal choice for this design.

Table 5. Weighting factors for different design responses.

Weighting Method	Quotas			
	Dis_1	Dis_2	*Cost*	*Mass*
FAHP	0.224167	0.210833	0.290833	0.274167
ICRITIC	0.190811	0.20895	0.31902	0.281228
FAHP-ICRITIC	0.207384	0.209885	0.305011	0.27772

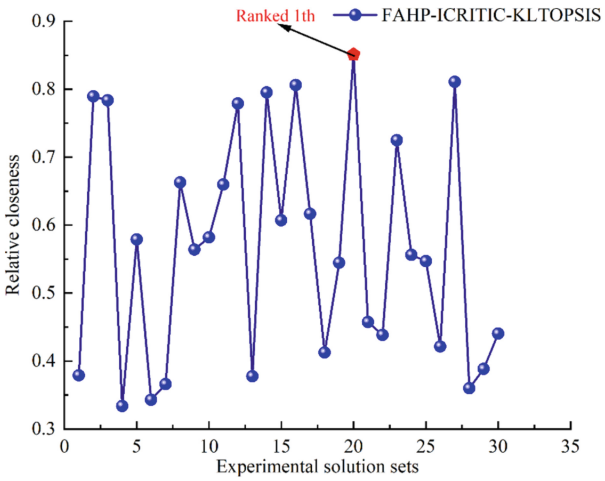

Fig. 4. Relative closeness of experimental solution sets obtained based on FAHP-ICRITIC-KLTOPSIS.

4 Conclusions

Table 6 presents a comparative analysis of the results before and after optimization. The optimized rear seat demonstrates a slight performance improvement, with reductions in mass and cost of 11.3% and 21.39%, respectively. Notably, the maximum deformation of the key measurement points on the headrest and backrest decreased by 1.37% and 2.45%, respectively. The optimized rear seats not only demonstrate a modest improvement in performance but also achieve a reduction in weight and cost. This indicates that the optimization strategy proposed in this paper is feasible and provides a reliable case study for related multi-objective optimization research. The optimized rear seats not only demonstrate a modest improvement in performance but also achieve a reduction in weight and cost. This indicates that the optimization strategy proposed in this paper is feasible and provides a reliable case study for related multi-objective optimization research.

Table 6. Weighting factors for different design responses.

Type	$Dis1$ (mm)	Dis_2 (mm)	*Cost* (¥/kg)	*Mass* (kg)
Responses	Min	Min	Min	Min
Original	75.23	62.47	53.08	11.08
Optimization	74.2	60.94	47.17	8.71
Improvement change(%)	1.37	2.45	11.13	21.39

5 Limitations

Although the finite element model in this paper has been experimentally validated, the final optimisation scheme has not yet been verified in actual production and experiments due to time and cost constraints. Cooperation with relevant companies will be sought to address this limitation in the future. As structural vibration fatigue and related factors tend to affect the service life of the seat, this paper suggests that subsequent optimisation studies should focus on a multi-objective design considering structural vibration fatigue, durability, and comfort, which will be a key aspect of future research.

References

1. Zhou, X., Jiang, H.L., Long, J.Q.: Multi-objective optimization design of rear seat for a passenger car based on GARS and NSGA-III. Proc. Inst. Mech. Eng. Part D J. Automob. Eng. 09544070241240168 (2024)
2. Shan, Z.Y., Long, J.Q., Yu, P., et al.: Lightweight optimization of passenger car seat frame based on grey relational analysis and optimized coefficient of variation. Struct. Multidiscip. Optim. **62**, 3429–3455 (2020)
3. Dai, C.X., Wang, X.C., Long, J.Q.: A new optimization strategy for multi-objective design of automotive seat frame. Struct. Multidiscip. Optim. **66**(11), 236 (2023)
4. Liao, Y.Q., Zheng, W., Long, J.Q., et al.: Ply optimization of backrest skeleton of carbon fiber reinforced plastic car seat based on grey euclidean relational analysis method. Int. J. Automot. Technol. **24**(4), 1189–1203 (2023)
5. Zhong, S.H., Chen, Y.Y., Miao, Y.J.: Using improved CRITIC method to evaluate thermal coal suppliers. Sci. Rep. **13**(1), 195 (2023)

Multi-axis Synchronous System Based on Adaptive S-Curve Algorithm

Jian Cui[1], Zhenyu Du[2(✉)], Nan Chen[2], Quanting Liu[1], Haoran Xu[1], Yuman Liu[1], Hongchen An[1], and Haolin Li[1]

[1] State Grid Jilin Electric Power Co., Ltd. Baishan Power Supply Company, Baishan, China
[2] Changchun University of Technology, Changchun, China
15843775789@163.com

Abstract. Aiming at the problem of system stability caused by poor synchronization of multi-axis control and excessive speed change in the control process, this paper proposes an adaptive S-curve algorithm based on the traditional S-curve, which can automatically adjust the value through the relationship between the two sides of the equation. The stability and effectiveness of this algorithm are verified by FPGA simulation. The synchronization of multi-axis control is verified by the test of CSV mode.

Keywords: S-curve · Multi-axis control · FPGA

1 Introduction and Optimization of S-Type Algorithm

1.1 Introduction of Traditional S-Type Algorithm

S-shaped acceleration and deceleration is a popular motion control algorithm at present. It is named because the speed curve of the controlled object in acceleration and deceleration stage is S-shaped. Common S-curves are parabolic and trigonometric. The core idea of S-curve algorithm is to make the acceleration not sudden change, so that the speed control of the controlled object has the characteristics of fast and stable [1]. This paper will take the parabola as an example to analyze the traditional S-curve, as shown in Fig. 1.

S-curve has seven stages of acceleration, uniform acceleration, deceleration, uniform speed, acceleration and deceleration, uniform deceleration and deceleration. Three key parameters need to be set to build an S-curve: maxv, maxa and J. maxv reflects the maximum operating capacity of the system, maxa reflects the maximum deceleration capacity of the system, and J reflects the flexibility of the system [2]. The greater the flexibility, the greater the overshoot and the shorter the running time.

1.2 Optimization of S-Type Acceleration and Deceleration Algorithm

In practice, different constraints will lead to changes in the motion process, resulting in different S-curves. Normally, a complete seven-segment S-curve can be formed only when the maximum speed is reached [3]. In practice, however, a complete seven-stage

J. Guo et al. (Eds.): MMTME 2024, 76, pp. 12–19, 2025.
https://doi.org/10.1007/978-981-96-5350-8_2

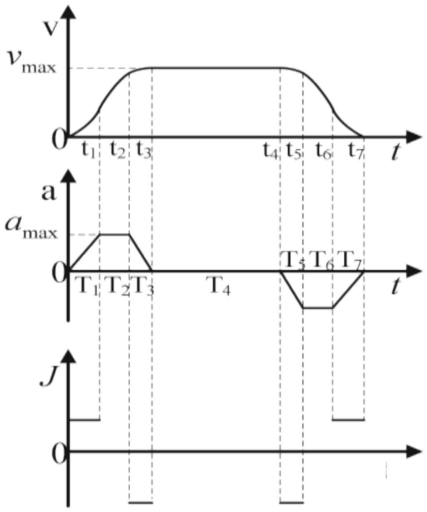

Fig. 1. Schematic diagram of 1S acceleration and deceleration curve

acceleration and deceleration curve cannot be generated because the maximum speed is sometimes not reached. To solve this problem, this paper introduces the concept of adaptive S-curve, assuming the existence of T2 and T6:

$$T_2 = T_6 = \frac{v_{\max} - v_S}{a_{\max}} - T_1 \tag{1}$$

$$T_4 = T_f - 2\frac{v_{\max}}{a_{\max}} - 2\frac{a_{\max}}{J} \tag{2}$$

$$J = \frac{a_{\max}^2 v_{\max}}{v_{\max} a_{\max} T_f - v_{\max}^2 - S a_{\max}} \tag{3}$$

In the running process, when T2 and T6 are greater than 0, it is a complete seven-segment S-curve; When T2 and T6 are less than 0, it is a five-stage S-curve; When T4 is also less than 0, it is a 4-section S-curve. The adaptive constraint formula is as follows:

$$\begin{cases} J = \dfrac{a^2 v}{T_f v a - v^2 - a} > 0 \\ t_2 = t_6 = \dfrac{2v}{a} + \dfrac{1}{v} - T \geq 0 \\ t_4 = \dfrac{2v}{a} - T \geq 0 \end{cases} \tag{4}$$

In the simulation software, the initial speed is assumed to be 0 by default, the termination speed is also 0, and the acceleration and deceleration regions are assumed to be symmetrical. Setting $ThetaStart = 0$, $ThetaEnd = 90$, $T_f = 1.8$. If the above inequality relationship is satisfied in the program, the operation can continue; If the above inequality relationship is not satisfied, the algorithm can automatically adjust the value. The program is written discretely.

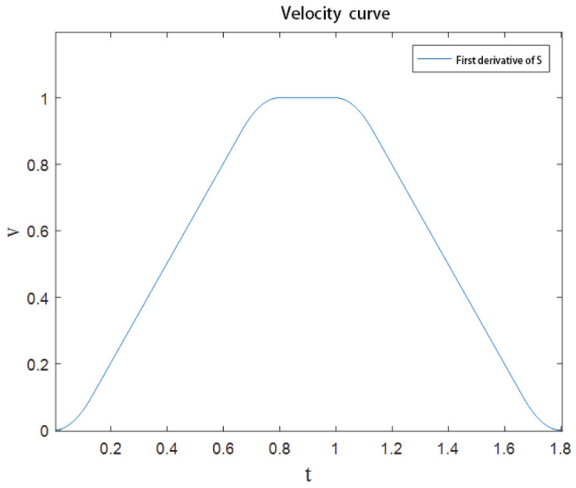

(a) Speed simulation curve

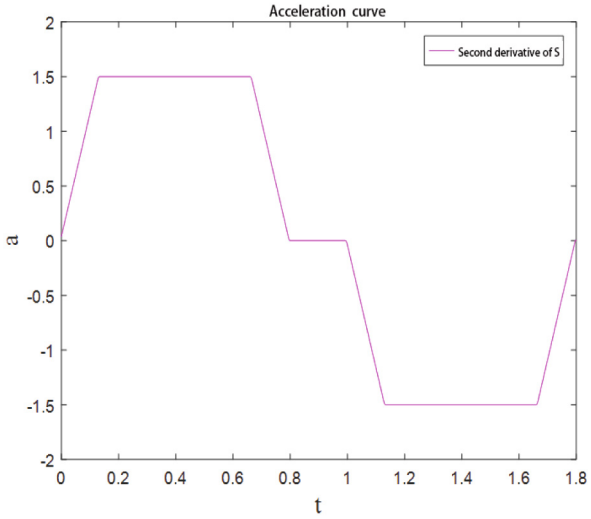

(b) Acceleration simulation curve

Fig. 2. Simulation of adaptive S-type acceleration and deceleration algorithm

As shown in the simulation analysis in Fig. 2, Fig. 2(a) speed simulation curve reflects continuous and smooth speed transformation, and Fig. 2(b) acceleration curve is continuous and stable, successfully avoiding abrupt phenomena during acceleration and deceleration. This strategy can identify the acceleration or deceleration state of S-curve by the application of constraint equation, and adjust the relevant parameters accordingly, which effectively weakens the instability of running time [4].

1.3 FPGA Simulation of Acceleration and Deceleration Algorithm

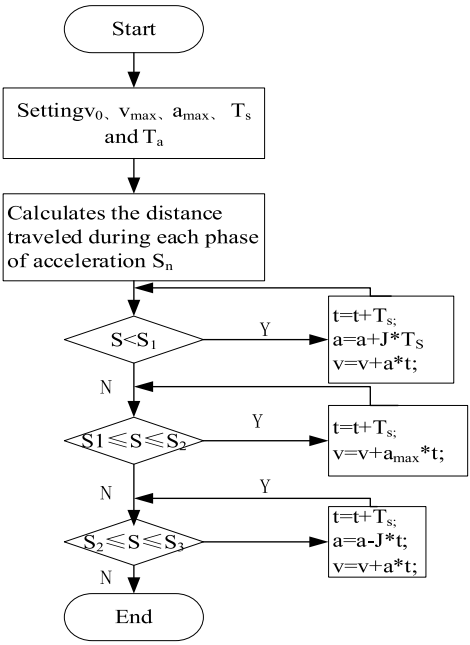

Fig. 3. Algorithm flow chart of acceleration stage

Because the motor has symmetry in the process of acceleration and deceleration, the time and movement distance required for acceleration and deceleration stages are the same [5]. Due to the large number of parameters in the algorithm and the complexity of calculation, the time can be used to infer whether the motor is in the acceleration, uniform acceleration or deceleration stage, and the constant period method is adopted for interpolation, that is, the acceleration and speed are calculated and modified every Tf time [7, 8]. The starting speed is set to 0v, the maximum speed is maxv, the maximum acceleration is maxa, and the acceleration time is Ta. The flow of the acceleration phase is shown in Fig. 3.

The interpolation time is set to 1ms, and the microcontroller adjusts the speed of the servo motor by changing the frequency of the output pulse signal, so the parameters of speed, acceleration and acceleration in the formula need to be converted into frequency units [6]. The detailed operations are as follows:

The implementation process of S-type acceleration and deceleration algorithm in FPGA is shown in Fig. 4. The specific process is as follows:

(1) Parameter determination. According to the electrical parameters of the selected servo motor and the load of each shaft, the starting speed frequency F0, the maximum speed frequency Fmax, the maximum acceleration frequency Fa and the acceleration time Ta are obtained through calculation and experiment. In order to ensure the speediness and stability of the motor, The value of Ta ranges from (0.05, 0.5).

```
assign  T_clk = 26'd50_000_000;
assign   CNT_up = (t_accel*T_clk)/100000; //acc time
assign   CNT_dn = (t_decel*T_clk)/100000; //dec time
assign  CNT_per= T_clk/speed_current;  //pulse out
assign  CNT_con= step_target - speed_target*(t_decel-t_decel/100)/2000;
//when dec time
assign  CNT_sup= speed_target*(t_accel-t_accel/100)/2000;
```

Fig. 4. Converts the parameters in the formula into frequency units

(2) Timer pulse frequency setting. By modifying the predivision coefficient and loading value of the general timer inside the controller, the output pulse frequency is modified. The calculation method is as follows:

$$F = \frac{T_{clk}}{(PCS + 1)(ARR + 1)} \tag{5}$$

In the formula, Tclk is the working clock frequency after frequency doubling, its value is 50MHz, and F is the timer interrupt trigger frequency.

(3) Calculation of interpolation steps. The overflows are measured by a universal timer inside the microcontroller, and an interpolation of velocity and acceleration is performed.

(4) Parameter modification. Input the moving distance S and calculate the total number of pulses PS required at this time. If the total number of pulses Pa in the acceleration stage conforms to Eq. (6),

$$P_a = \frac{F_0 + F_m}{2} T_a \leq \frac{P_S}{2} \tag{6}$$

Then the acceleration stage of step (5) is entered, and conversely, Fmax is reduced until the total number of pulses Pa in the acceleration stage conforms to formula (6).

(5) Acceleration stage. Turn on the pulse output timer and the interpolation timer, and the motor moves in the acceleration phase.

Uniform speed stage. When the motor motion pulse number $P = P_a$, the motor completes the acceleration of the current stage and begins to move at a constant speed. When the motor pulse number $P = P_S - P_a$, the motor begins to carry out the deceleration phase.

(6) Deceleration stage. Motor deceleration, when the motor pulse number $P = P_S$, stop sending pulses, motor stop.

Figure 5 shows the flow chart of the S acceleration and deceleration FPGA program.

The simulation results of the S-type acceleration and deceleration module were shown in Fig. 6. As can be seen from the figure, the output pulse speed_current presents obvious acceleration and deceleration characteristics. The actual acceleration time is 297ms, the deceleration time is 396ms, and the pulse number at the constant speed stage is 500. When the output pulse number is 64,000, the speed_current decelerates exactly to 0 and the motor stops, which meets the design requirements [9, 10].

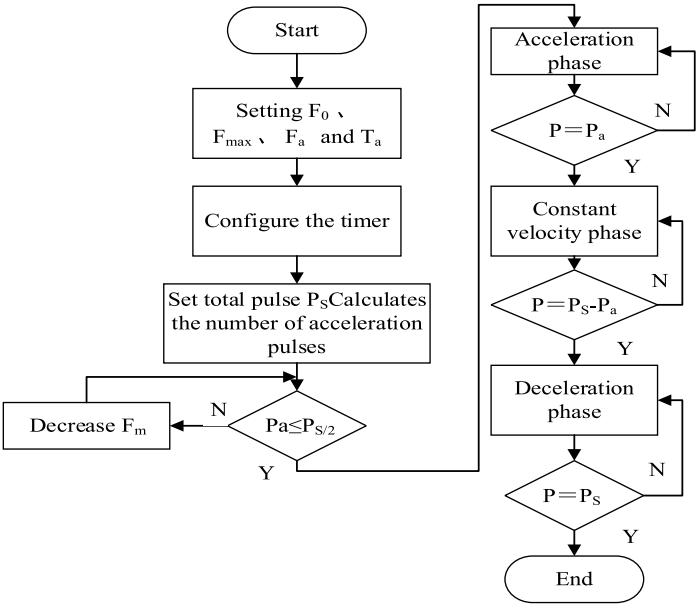

Fig. 5. S acceleration and deceleration FPGA program flow chart

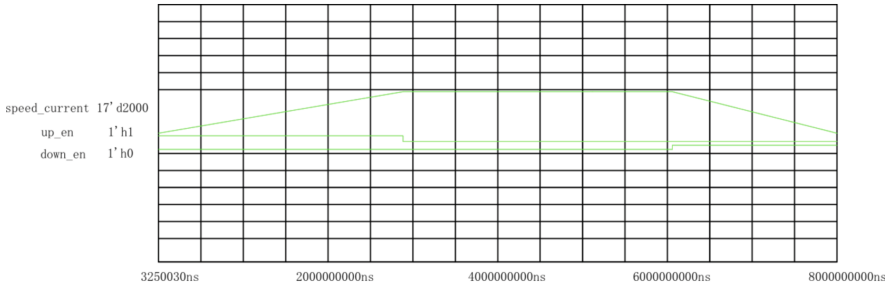

Fig. 6. FPGA simulation of adaptive S-type acceleration and deceleration algorithm

Figure 7 shows the waveform of the real-time speed curve of the motor under test in CSV mode. The experimental platform was set up as shown in Fig. 8, and the oscilloscope was used to capture the Sync synchronization signal of the X axis and the Y axis to execute an action command at the same time, and the experiment was carried out several times, and one of the experimental results was taken as shown in Fig. 9.

As can be seen from Fig. 9, when the process data period is set to 1ms, the measured two-axis action time interval is 810ns, and the fluctuation is only in the nanosecond range, indicating that the system has high synchronization performance in X/Y axis synchronization.

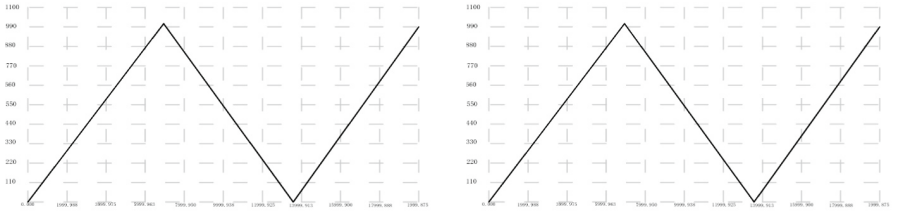

(a) X-axis velocity curve waveform (b) Y-axis velocity curve waveform

Fig. 7. Waveform of the real-time speed curve of the motor under the test in CSV mode

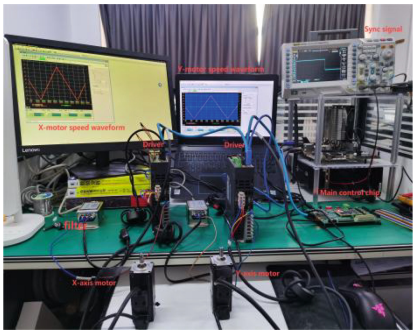

Fig. 8. Experimental platform construction

Fig. 9. Waveform of X/Y axis Sync0 signal

2 Closing Remarks

This paper is based on the adaptive S-curve algorithm, the method is simple, and compared with the traditional S-curve algorithm, the limitation is smaller, and the accuracy is of great significance for avoiding the mechanical rigidity consumption, synchronization and accuracy. The smooth trajectory without impact is guaranteed, which proves the effectiveness of this method in the multi-degree-of-freedom control system.